Directional Solidification in Two and Three Dimensions

Bruno Grossmann,[1] K. R. Elder,[2] Martin Grant,[2] and J. M. Kosterlitz[1]
[1]*Department of Physics, Brown University, Barus and Holley Building, Providence, Rhode Island 02906*
[2]*Department of Physics, McGill University, Rutherford Building, 3600 University Street, Montréal, Québec, Canada H3A 2T8*
(Received 23 July 1992)

A symmetric phase-field model is used to study directional solidification in two and three dimensions. Numerical evidence of tip-splitting, breathing modes, solitary modes, and other non-steady-state behavior is seen in 2D. A simple model for the breathing modes is proposed. Finally, 3D simulations indicate a hexagonal ordering of cells.

PACS numbers: 64.60.Ht, 05.40+j, 05.70.Ln, 68.35.Fx

The process of directional solidification provides an interesting example of nonlinear nonequilibrium physics [1–14]. In a typical experiment a liquid is pulled through a temperature gradient G at a constant velocity v such that behind (ahead of) this gradient a solid (liquid) phase is stable. When the chemical composition of the two phases is different at coexistence, the liquid/solid interface develops a steady-state periodic cellular structure for a range of v and G, while non-steady-state interfaces display many interesting phenomena [1,3–6,10,12,14], including tip splitting, pinching, breathing, and solitary modes. In this paper we introduce a phase-field model to study numerically directional solidification in 2D and 3D. The motivation is to show that the model contains the correct physics, has the mathematical simplicity to make numerical simulations feasible and to provide new insight into some non-steady-state phenomena.

The phase-field model we propose is an extension of the one developed for solidification processes [15]. The phenomenology that enters this model is at the level of phase fields and does not require such approximations [2,8,9,11,13,14] as the quasistationary approximation and the infinitely thin liquid/solid interface limit that enter sharp interface models. Nevertheless, the phase-field model reduces to the sharp interface equations in the appropriate limit. The free energy can be written as

$$\mathcal{F}=\int d\mathbf{x}\left[\frac{1}{2}D_\phi|\nabla\phi|^2+\frac{1}{4}\beta(\phi^2-1)^2+\frac{1}{2}\gamma\Delta\phi U^2+\Delta T\phi\right]. \tag{1}$$

Here, ϕ is a nonconserved field describing the liquid/solid transition, $U \equiv c + \phi/\Delta\phi$, c is a dimensionless diffusion field proportional to the impurity concentration, and $\Delta T \equiv T - T_m$, where T is proportional to temperature and T_m to the melting temperature. $\Delta\phi$ is the miscibility gap and D_ϕ, β, and γ are phenomenological constants [15]. The dynamics of these fields can be written $\partial\phi/\partial t = -\Gamma_\phi\delta\mathcal{F}/\delta\phi$ and $\partial c/\partial t = \Gamma_c/(\gamma\Delta\phi)\nabla^2(\delta F/\delta c)$, where Γ_ϕ and Γ_c are the mobilities of ϕ and c, respectively. For simplicity, a symmetric model is considered where the mobilities are independent of ϕ. In a frame moving in the $\hat{\mathbf{z}}$ direction at speed v, the dynamics can be written as

$$d\phi/d\tau = D_\phi\nabla^2\phi + \beta(\phi-\phi^3) - \gamma U - \Delta T(z'), \tag{2}$$

$$dU/d\tau = D_U\nabla^2 U + (d\phi/d\tau)/\Delta\phi, \tag{3}$$

where $z' \equiv z - v\tau$, $d/d\tau \equiv \partial/\partial\tau - v\partial/\partial z'$, $D_U \equiv \Gamma_c/\Gamma_\phi$, and $\tau \equiv \Gamma_\phi t$. The moving temperature gradient is implemented by $\Delta T(z')$ with $\Delta T = -\Delta T_o$ for $z' < -W$, $z'G$ for $|z'| < W$ and ΔT_0 for $z' > W$, where $G \equiv \Delta T_0/W$. The average impurity concentration is taken to be $c_0 = 0$ and $\Delta T_0 > \gamma/\Delta\phi$ so that the temperature $\Delta T(z')$ is above (below) the liquidus (solidus) line for $z' > W$ ($z' < -W$). In this model the partition coefficient is 1.

The 2D sharp interface equations [2,8,9,11,13,14] can be easily obtained using standard methods [15–19] from Eqs. (2) and (3). Far from the interface, $|z'| >> W$, $d\phi/d\tau$ is negligible so that $v\partial U/\partial z' + D_U\nabla^2 U = 0$. One boundary condition can be obtained by integrating Eq. (3) across the interface to give, in the limit of a sharp interface, $(v+\zeta_\tau)\hat{\mathbf{n}}\cdot\hat{\mathbf{z}} = D_U(\boldsymbol{\nabla}U|_s - \boldsymbol{\nabla}U|_l)\cdot\hat{\mathbf{n}}$. Here, $\hat{\mathbf{n}}$ is the direction normal to the interface position (ζ), which is defined by $\phi(z'=\zeta)=0$, and the subscripts l and s refer to the liquid and solid sides of the interface, respectively. To obtain the Gibbs-Thomson condition, we write $\phi = \phi^{1D} + \delta\phi$ where ϕ^{1D} satisfies $D_\phi\nabla^2\phi^{1D} + \beta[\phi^{1D} - (\phi^{1D})^3] = 0$ and introduce a coordinate u along $\hat{\mathbf{n}}$. Integrating Eq. (2) over $\partial\phi^{1D}/\partial u$ gives $U(w=0) - (1+U_\infty) = -d_0\kappa - \zeta/l_T$, where $d_0 \equiv \sigma/2\gamma$, $\sigma \equiv D_\phi\int du(\partial\phi^{1D}/\partial u)^2$, $l_T \equiv \gamma/G$, and κ is the curvature. This equation was obtained by expanding to lowest order in κ and ignoring the time dependence of w and $\delta\phi$. The diffusion equation and the two boundary conditions form the basis of the sharp interface model of directional solidification.

Numerical simulations of Eqs. (2) and (3) were performed on a discrete lattice with free boundary conditions in the $\hat{\mathbf{z}}$ direction and periodic in the others. A nearest-neighbor Laplacian and Euler's method for the time derivatives was used. The mesh size was 1.0 and the time step was 0.1. To begin each simulation 1D solutions (i.e., ϕ^{1D} and U^{1D}) were obtained numerically and the initial state was set to $\phi(x,z') = \phi^{1D}(x, z' - \zeta(x,0))$ and $U(x,z') = U^{1D}(x, z' - \zeta(x,0))$. For all the simulations presented, $\beta = 1$ and $\Delta T_0 = 0.38$. The parameter

set $(L_x, L_z, \gamma, D_\phi, D_U, W, v)$ and $\zeta(x,0)$ will be specified for the individual simulations discussed below. The parameters were chosen so that the ratios l_T/l and l/d_0 ($l \equiv 2D_U/v$) are similar to those in recent experiments [1,5] on the liquid crystal 4-n-octylcyanobiphenyl (8CB).

The first simulations were conducted to analyze the stability of a planar interface to small perturbations. For this test, $\zeta(x,0) = A_0\cos(kx)$ and the parameter set was $(2\pi/k, 150, 0.73, 1.5, 2, 50, 0.2)$. By fitting $\zeta(x,\tau)$ with $A_0 e^{\omega(k)\tau}\cos(kx)$, an estimate of the linear dispersion relationship $\omega_l(k)$ was obtained. In Fig. 1 the numerical results are shown to be quite close to the predictions [8] of the sharp interface model: $\omega_s(k) = v[\sqrt{1+(kl)^2}(1 - l/l_T - d_0 l k^2) - 1]/l$. For the same parameter set, with $L_x = 1000$ and $\zeta(x,0)$ unit amplitude white noise, a stationary solution was obtained as shown in the inset of Fig. 1 in both real and Fourier space, $\zeta(k) \equiv \int dx\, e^{ikx}\zeta(x)$.

Various non-steady-state effects were seen (Fig. 2) as observed in experiments [1,3–6] and simulation [10]. The tip-splitting instability shown in Fig. 2(a) was obtained by increasing the velocity from $v = 0.2$ to 0.4 over a time $\tau = 5$ with parameters $(500, 163, 0.72, 1.5, 1, 25, 0.2 \to 0.4)$. Two colliding solitary modes can be seen in Fig. 2(b) obtained by an instantaneous velocity jump from $v = 0.5$ to 0.3 for the set $(500, 221, 0.4, 1.5, 1, 25, 0.5 \to 0.3)$. Other exotic patterns were formed during velocity changes, one example as shown in Fig. 2(c) in which the velocity was increased from 0.03 to 0.07 over a time range of 40 for the set $(500, 163, 0.72, 1.5, 1, 200, 0.03 \to 0.07)$.

Breathing modes were observed in a variety of ways. A slight increase in the pulling velocity sometimes created small regions of collective oscillations. They were also generated by an x-dependent temperature gradient, $\Delta T(z' - f(x))$, where $f(x) = 1.61 \times 10^{-5}x^2 - 0.008x + 0.008$. For the set $(500, 175, 0.63, 1.5, 1, 50, 0.2)$ and a random initial interface, a collective breathing state emerged. Breathing modes were also created by an initial configuration of the form $\zeta(x,0) = \cos(24\pi x/L_x) + \cos(12\pi x/L_x)$, as shown in Fig. 2(d) for the set $(495, 175, 0.63, 1.5, 1, 50, 0.2)$. They were also obtained using the same parameter set and random $\zeta(x,0)$.

To understand the breathing modes we propose a simple model for the positions of the grooves. The nth groove is at $x = u_n$, defined by $\zeta_x|_{u_n} = 0$ and $\zeta_{xx}|_{u_n} > 0$. We explicitly assume breathing modes exist and do not attempt to study the instability that creates them [14]. Following the idea that all forces are thermodynamic, we assume the grooves can be treated as particles with a force F acting between them, determined by the change in free energy density ΔE for a uniform expansion or contraction of the steady-state interface shape $\zeta^{ss}(x)$. The important contributions to the free energy of the interface come from gradients in ϕ and c, which we approximate to be $|\nabla\phi(z' - \zeta(x,\tau))|^2 = (1+\zeta_x^2)|d\phi/dw|^2$ and similarly for c. Thus, ΔE is of the form $\Delta E \approx E_C\lambda^{-1}\int_0^\lambda dx|\zeta_x^{ss}(x)|^2 - [\lambda(1+\epsilon)]^{-1}\int_0^{\lambda(1+\epsilon)} dx|\zeta_x^{ss}(x/(1+\epsilon))|^2]$ where λ is the average groove spacing, $1+\epsilon$ is the fractional expansion, and E_C is a linear combination of $\int_{-\infty}^{\infty} dw|d\phi/dw|^2$ and $\int_{-\infty}^{\infty} dw|dU/dw|^2$. Using $F\epsilon\lambda = \Delta E$ and considering expansions or contractions due to u_{n+1} and u_{n-1}, we obtain

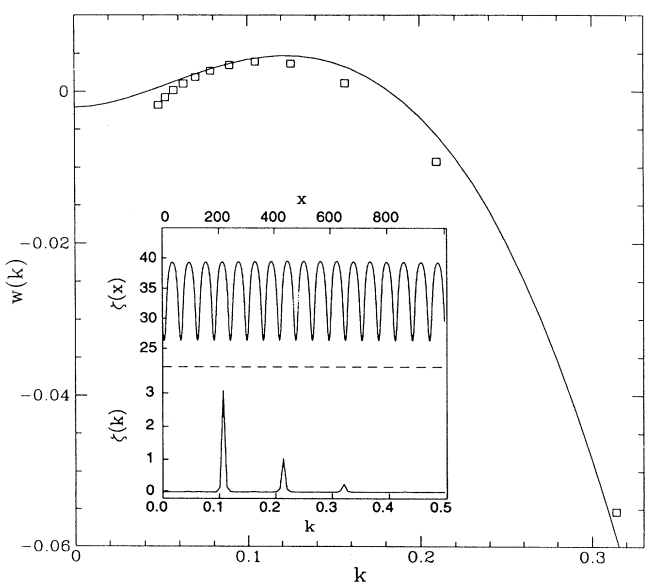

FIG. 1. Linear dispersion relation around a planar interface. The points correspond to numerical integration of Eqs. (2) and (3) and the solid line corresponds to the sharp interface result $[\omega_s(k)]$ given in the text. Inset: Stationary interface in real and Fourier space.

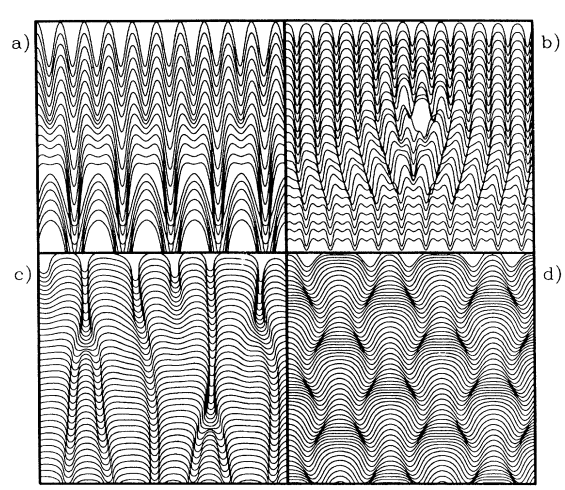

FIG. 2. Non-steady-state interfaces from Eqs. (2) and (3). Tip splitting (a); collision of two solitary modes (b); exotic pattern (c); and breathing modes (d). The (x, y) axes are (distance, time) of (200, 1900) (a), (400, 2500) (b), (500, 8400) (c), and (200, 13 750) (d).

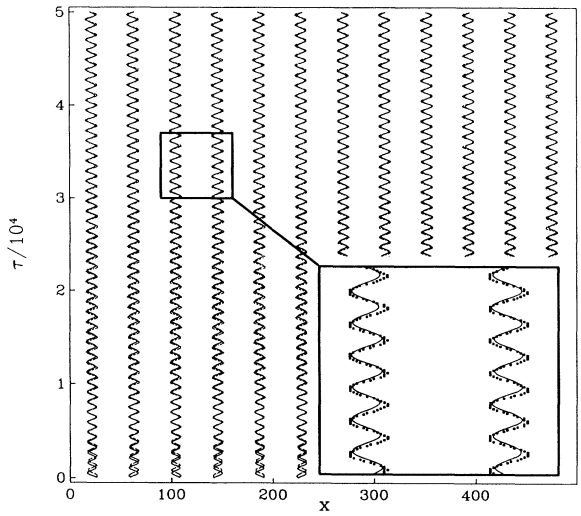

FIG. 3. Groove positions $\{u_n\}$ as function of time from Eqs. (2) and (3) (points) and Eq. (4) (lines). The (distance, time) spanned is (500, 250 000). Inset: Comparison of results for box region.

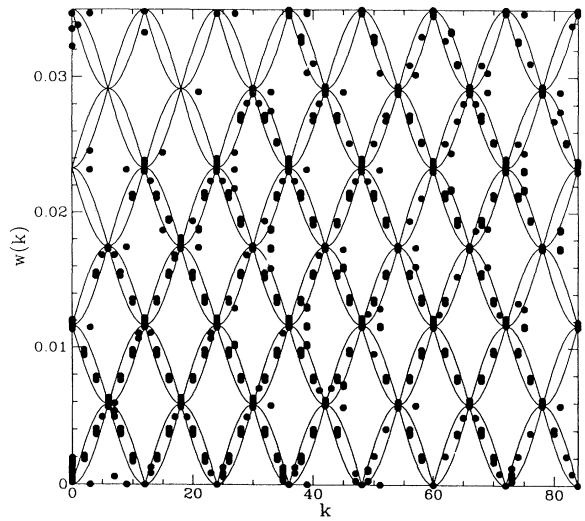

FIG. 4. Dispersion relation from simulation of Eq. (4) compared to that from phase-field model. The points are the peaks of $S(k,\omega)$ obtained from phase field model and the lines $[\omega(k)]$ were obtained from the groove dynamics.

$$\partial^2 v_n/\partial t'^2 = C\,[(2+v_n-v_{n-1})/(1+v_n-v_{n-1})^2 - (2+v_{n+1}-v_n)/(1+v_{n+1}-v_n)^2], \quad (4)$$

with $C \propto E_C\lambda^{-1}\int_0^\lambda dx|\zeta_x^{ss}|^2$, $u_n \equiv \lambda(n+v_n)$, and $t' \equiv \tau/\lambda$. Equation (4) was simulated with the initial set of groove positions taken directly from the numerical simulation, and C was adjusted to obtain the best fit to the numerical data from phase-field simulations. A comparision is shown in Fig. 3. This calculation is equivalent to expanding the force on the nth groove to lowest order in curvature which is assumed to be inversely proportional to the distance between grooves. It can also be written $F_n = A(\kappa_n - \kappa_{n+1}) + \cdots$, where κ_n is the average curvature of the nth and $(n-1)$th grooves.

Equation (4) is equivalent to particles with equilibrium positions $v_n = 0$ connected by very anharmonic springs. A linear analysis gives $\omega_{ac} = 2\sqrt{C}|\sin(k/2)|$ which is identical to an acoustic mode in a monatomic Bravais lattice. The influence of the anharmonicity was studied by simulation from an initial state given by $v_n = \epsilon_n + 0.1\cos\pi n$ where ϵ_n is a random number with $|\epsilon_n| < 0.3$. A system of 512 grooves with periodic boundary conditions on v_n was averaged over 10^4 runs. The peaks in the dynamic structure factor $S(k,\omega) \equiv \langle|v(k,\omega)|^2\rangle$, with $v(k,\omega) = \int dt \sum_n v_n(t)\exp i(2\pi nk/512 + \omega t)$, occur at $\omega = 2\sqrt{C}[2m \pm |\sin(k/2)|]$ and at $\omega = 2\sqrt{C}[2m+1 \pm |\cos(k/2)|]$ for $m = 0, \pm1, \pm2, \ldots$. The largest of these are at zone boundaries, $k = \pi$, corresponding to breathing modes of frequency $\omega_b = 2\sqrt{C}$. Since $t' = \tau/\lambda$, we obtain the result that $\omega_b \propto \lambda^{-1}$. This relation was observed in experiments on a cholesteric/isotropic interface [3] where coupling to the helical pitch plays an important role. In Fig. 4 the dispersion relation obtained from Eq. (4) is compared with that obtained from the phase field equations with satisfactory agreement.

To illustrate the advantages of a phase-field model, a 3D simulation was done on a cubic lattice with the parameters given by a linear stability analysis. $L_x = L_y = L_z = 100$ and $\zeta(x,y,0)$ is white noise of unit amplitude. Figure 5 shows a contour plot of ζ after a steady state was reached and hexagonal ordering of the cells is clearly

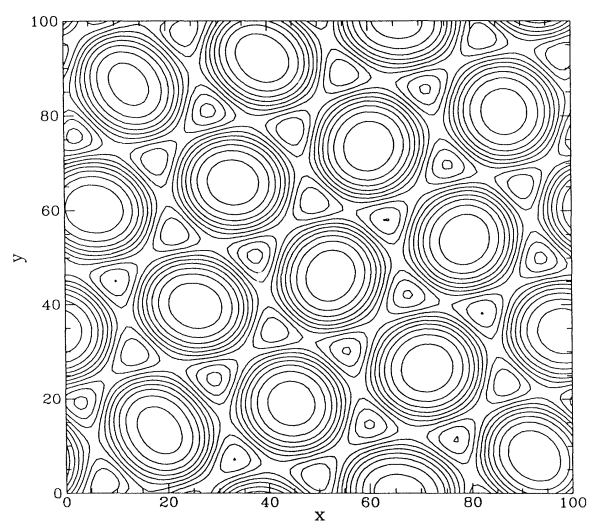

FIG. 5. Contour plot, $|\zeta| \leq 2.5$ in steps of 0.5, of 2D interface in 3D system. The large circular contours correspond to "hills" and the smaller triangular contours to "valleys."

seen which is consistent with experiment [7] and theoretical expectations [9].

In summary, the usefulness of a full phase-field model in examining the behavior of directional ordering is established. The model is consistent with the sharp interface equations in the appropriate limit and reproduces many non-steady-state phenomena. New insight into the phenomena of breathing modes was discovered, leading to a prediction for the full dispersion relation. We hope these results will provide the stimulus for future experiments.

One of us (B.G.) is grateful to André Vallat for interesting discussions. This work was supported by the Natural Sciences and Engineering Research Council of Canada, and le Fonds pour la Formation de Chercheurs et l'Aide à la Recherche de la Province de Québec. J.M.K. was partially supported by NSF Grant No. DMR-9222812.

[1] J.-M. Flesselles, A.J. Simon, and A.J. Libchaber, Adv. Phys. **40**, 1 (1991), and references therein.
[2] J.S. Langer, Rev. Mod. Phys. **52**, 1 (1980).
[3] P.E. Cladis, "Pattern Formation at the Cholesteric-Isotropic Interface" (to be published); P.E. Cladis, J.T. Gleeson, P.L. Finn, and H.R. Brand, Phys. Rev. Lett. **67**, 3239 (1991)
[4] P.E. Cladis, J.T. Gleeson, and P.L. Finn, in *Patterns, Defects and Materials Instabilities*, edited by D. Walgraef and N.M. Ghoniem (Kluwer Academic Publishers, Dordrecht, The Netherlands, 1989), pp. 135-146.
[5] A. J. Simon, J. Bechhoefer, and A. Libchaber, Phys. Rev. Lett. **61**, 2574 (1988).
[6] P. Oswald, J. Bechhoefer, and A. Libchaber, Phys. Rev. Lett. **58**, 2318 (1987).
[7] H. Biloni, G.F. Bolling, and G.S. Cole, Trans. AIME **236**, 930 (1966).
[8] W.W. Mullins and R.F. Sekerka, J. Appl. Phys. **35**, 444 (1964).
[9] D.J. Wollkind and L.A. Segel, Philos Trans. R. Soc. London A **268**, 351 (1970).
[10] K. Kassner, C. Misbah, and H. Müller-Krumbhaar, Phys. Rev. Lett. **67**, 1551 (1991).
[11] K. Brattkus and C. Misbah, Phys. Rev. Lett. **64**, 1935 (1990).
[12] P. Coullet, R. Goldstein, and G. H. Gunaratne, Phys. Rev. Lett. **63**, 1954 (1989).
[13] Y. Saito, C. Misbah, and H. Müller-Krumbhaar, Phys. Rev. Lett. **63**, 2377 (1989).
[14] W-J Rappel and H. Riecke, Phys. Rev. A **45**, 846 (1992).
[15] J.B. Collins and H. Levine, Phys. Rev. B **31**, 6119 (1985); J.B. Collins, A. Chakrabarti, and J.D. Gunton, Phys. Rev. B **39**, 1506 (1989).
[16] J. Langer, in *Directions in Condensed Matter Physics* edited by G. Mazenko and G. Grinstein (World Scientific, Singapore, 1986), p. 165ff.
[17] G. Caginalp, Phys. Rev. A **39**, 5887 (1989).
[18] H. Löwen, J. Bechhoefer, and L. S. Tuckerman, Phys. Rev. A **45**, 2399 (1992).
[19] A. A. Wheeler, W. J. Boettinger, and G. B. McFadden, Phys. Rev. A **45**, 7424 (1992).